Interfacial dislocations in (111) oriented $(Ba_{0.7}Sr_{0.3})TiO_3$ films on $SrTiO_3$ single crystal

Xuan Shen,[1,2] Tomoaki Yamada,[3,4,5] Ruoqian Lin,[2] Takafumi Kamo,[5] Hiroshi Funakubo,[5] Di Wu,[1] Huolin L. Xin,[2] and Dong Su[2]*

1. National Laboratory of Solid State Microstructures, Department of Materials Science and Engineering, College of Engineering and Applied Science, and Collaborative Center of Advanced Materials, Nanjing University, Nanjing, 210093, China.

2. Center for Functional Nanomaterials, Brookhaven National Laboratory, Upton, NY 11973, USA.

3. Department of Materials, Physics and Energy Engineering, Nagoya University, Furo-cho, Chikusa-ku, Nagoya 464-8603, Japan.

4. PRESTO, Japan Science and Technology Agency, 4-1-8 Honcho, Kawaguchi, Saitama 332-0012, Japan.

5. Department of Innovative and Engineered Materials, Tokyo Institute of Technology, Yokohama 226-8502, Japan.

Abstract

We have investigated the interfacial structure of epitaxial $(Ba,Sr)TiO_3$ films grown on (111)-oriented $SrTiO_3$ single-crystal substrates using transmission electron microscopy (TEM) techniques. Compared with the (100) epitaxial perovskite films, we observe dominant dislocation half-loop with Burgers vectors of $\boldsymbol{a}$<110> comprised of a misfit dislocation along <112>, and a threading dislocation along <110>. The misfit dislocation with Burgers vector of $\boldsymbol{a}$<110> can dissociate into two ½$\boldsymbol{a}$<110> partial dislocations and one stacking fault. We found the dislocation reactions occur not only between misfit dislocations, but also between threading dislocations. Via three-dimensional electron tomography, we retrieved the configurations of the threading dislocation reactions. The reactions between threading dislocations lead to a more efficient strain relaxation than do the misfit dislocations alone in the near-interface region of the (111)-oriented $(Ba_{0.7}Sr_{0.3})TiO_3$ films.

* Electronic mail: dsu@bnl.gov

Perovskite oxide films have been studied intensively for their promising applications in integrated dynamic random access memories (DRAMs), microwave tunable devices, and high-k capacitors, due to their excellent dielectric and ferroelectric properties.[1-6] It was demonstrated, both theoretically and experimentally, that interfacial stresses and defect structures strongly influence the films' dielectric and ferroelectric properties.[7-12] On the other hand, according to the Matthews-Blakeslee model,[13,14] interfacial dislocations form to relax the elastic strain in epitaxial films when the film's thickness exceeds a critical value. Structural investigations were undertaken on strain relaxation and the defect structures, especially on the mechanism for accommodating misfit strains through the nucleation and growth of dislocations. For example, Suzuki and his coworkers observed major misfit dislocations with Burgers vectors of type $\boldsymbol{a}$<100>, and threading dislocations with Burgers vectors of type $\boldsymbol{a}$<110> in (001) $BaTiO_3/SrTiO_3$ thin films.[15] Similar investigations were undertaken in other {100}-oriented epitaxial films, such as $SrTiO_3/LaAlO_3$,[16,17] $(Ba,Sr)TiO_3/LaAlO_3$,[18,19] and $Pb(Zr,Ti)O_3/SrTiO_3$[20,21]. For a (001)-oriented perovskite epitaxial thin film, misfit/threading dislocations with Burgers vectors of $\boldsymbol{a}$<100> and ½$\boldsymbol{a}$<110> were identified as major dislocations, and a dislocation half-loop mechanism accounted for their formation. However, up to now, most such studies have focused on (001)-oriented epitaxial films, not on other orientations, even though strain relaxation behavior may be influenced by different orientations that directly affect the films' dielectric and ferroelectric properties.[22] This omission motivated us to characterize the interfacial structure and dislocations in (111)-oriented BST thin films.

Using combined transmission electron microscopy (TEM) approaches, including electron diffraction, scanning transmission electron microscopy (STEM), electron energy loss spectroscopy (EELS), and high resolution-TEM (HRTEM), we investigate the interfacial structure of epitaxial $(Ba_{0.7}Sr_{0.3})TiO_3$ (BST) thin films deposited on (111) $SrTiO_3$ (STO) single crystal substrates and with electron tomography, we further visualized the three-dimensional (3D) morphology of the threading dislocations. We compare the configurations of misfit and threading dislocations in (111) BST films with those in (100) BST thin films grown under the same conditions. Our results can be applied to other {111} epitaxial perovskite-film systems to help in understanding their mechanisms of strain relaxation.

The (111)-oriented epitaxial BST films (~ 10 and ~ 300 nm, respectively) were deposited on the (111) STO substrates, by rf magnetron sputtering at 700 ^{o}C. The crystallinity of the films was confirmed by X-ray diffraction (XRD). The results of reciprocal space mapping suggested that the in-plane lattice parameters for the 300 nm-thick films are close to their bulk values, meaning that the film is almost fully relaxed. Details of the growth and dielectric properties of the BST films are given elsewhere.[23] The

cross-sectional TEM specimens were prepared using Ar-ion milling after applying a wedge-polishing method. The sample for electron tomography was prepared by the focused ion beam (FIB) lift-out technique, using the FEI-Helios FIB system. We employed a 2 kV Ga-ion beam for final thinning to remove the damaged layer at the surface. A plane-view specimen was prepared by cutting into a 3 mm diameter disk, followed by mechanical grinding, and subsequently by Ar-ion milling on the substrate side using a Gatan-PIPS. STEM-EELS characterization of the BST/STO heterostructure was undertaken under an aberration-corrected Hitachi HD2700C dedicated STEM, equipped with a high-resolution parallel EELS detector (Gatan Enfina-ER). HRTEM images, electron diffraction patterns, and electron tomography were obtained with a JEOL JEM2100F TEM, operated at 200 kV.

We first characterized a ~ 10 nm thick BST film along the plane-view using TEM and STEM-EELS. Fig. 1 (a) is the SAED pattern from the plane-view sample containing both BST and STO. An exact coincidence is evident from their [111] diffraction patterns with hexagonal symmetry, indicating that their in-plane lattices are coherent. A bright-field TEM image obtained using a diffraction vector $\boldsymbol{g} = 10\bar{1}$ under the two-beam condition is shown in Fig. 1 (b). We observed two arrays of misfit dislocations (straight lines) crossing each other, and aligned along the $[2\bar{1}\bar{1}]$ and $[11\bar{2}]$ directions. As described in the following paragraph, we identified them as pure edge dislocations with Burgers vectors of either $\boldsymbol{a}$<110> or 1/2$\boldsymbol{a}$<110>. As shown in Fig. 1(c), at some end points, the misfit dislocations have reacted to form threading dislocations (short curved segments), as marked with the blue square.[24,25] In contrast, another misfit dislocations can directly change into threading dislocations, as marked with the green square.[15,26] These findings suggest that the dislocations have formed half-loops. The threading dislocation lines occur along the <110> direction. Interestingly, similar dislocations are also observed in plane-view samples of (001)-oriented BST/STO deposited under the same conditions, as shown in Fig. S1. Fig. 1 (d) shows the selected area electron diffraction (SAED) pattern along the $[11\bar{2}]$ zone axis from a cross-sectional sample. It was confirmed that the BST film grew epitaxially on the STO substrate with a crystallographic relation of $(111)[111]_{BST}//(111)[111]_{STO}$, in accord with the XRD results.[23] The STEM-EELS line scan shown in Fig. S2 suggest that there is an abrupt interface between the BST film and the STO substrate, oriented along [111] direction. Also, as indicated by the white dashed square in Fig. 1 (d), a slightly splitting of $\boldsymbol{g}_{BST}(\bar{2}\bar{2}\bar{2})$ and $\boldsymbol{g}_{STO}(\bar{2}\bar{2}\bar{2})$ is observed from the diffraction pattern which indicates the clamping effect resulting from the lattice mismatch between the film and substrate. According to the Matthews-Blakeslee model,[13,14] the critical thickness, $\boldsymbol{h_c}$ can be expressed as

$$\boldsymbol{h_c} = \frac{b}{4\pi\sigma(1+\nu)}\left[ln\left(\frac{\boldsymbol{h_c}}{b}\right)+1\right]; \qquad (1)$$

where σ is the lattice mismatch, v represents the Poisson's ratio, and $\boldsymbol{b}$ is the Burgers vector of the misfit dislocation. The Poisson's ratio of BST is estimated at about 0.31, using the average value of STO and $BaTiO_3$ (BTO).[27,28] The lattice mismatch between these two materials (the bulk lattice parameter of BST is weight-averaged by the composition ratio of STO and BTO, as 3:7) is about 1.7%, resulting in a compressive strain in the epitaxial films. The critical thickness of (111)-oriented BST/STO then is estimated to be 3.6 nm thinner than that of (001)-oriented one, at 5.0 nm. This difference would result in a faster strain relaxation in (111)-oriented BST films, as discussed previously in Ref. 23. As shown in the HRTEM image along $[11\bar{2}]$ zone axis in Fig. 1 (e), the Burgers vector of the misfit dislocations is identified along $[1\bar{1}0]$. We can not identify its Burgers vector because at the $(11\bar{2})$ plane, the one unit cell's shift can be either from Burgers vector of $\frac{1}{2}\boldsymbol{a}[1\bar{1}0]$ or $\boldsymbol{a}[01\bar{1}]$, as shown in Fig. 1 (g). On the other hand, those two Burgers vectors can be distinguished from <110> zone axis. To help understand the geometry of the Burgers vectors, the schematic of $(11\bar{2})$ and $(1\bar{1}0)$ planes are shown in Fig. S3 (a) and (b). As shown in Fig. 1 (f), we observed two misfit dislocations with Burgers vectors of $\boldsymbol{a}[01\bar{1}]$ and $\frac{1}{2}\boldsymbol{a}[110]$, respectively. According to Frank's rule[29] (i.e., the energy of an elastic strain associated with dislocations is proportional to the square of its Burgers vector), the elastic strain energy of $\boldsymbol{a}[1\bar{1}0]$ dislocation can be reduced when dissociating into two $\frac{1}{2}\boldsymbol{a}[1\bar{1}0]$ partial dislocations, as shown in EQ (2). Whereas during this dissociation, a stacking fault (SF) with the same translation vector as $\frac{1}{2}\boldsymbol{a}[1\bar{1}0]$ is formed, increasing a stacking fault energy. This reaction can interpret the formation of $\frac{1}{2}\boldsymbol{a}[110]$ partial dislocations and the stacking faults observed in Fig. 1 (f) and Fig. S4.

$$\boldsymbol{a}[1\bar{1}0] = \tfrac{1}{2}\boldsymbol{a}[1\bar{1}0] + \tfrac{1}{2}\boldsymbol{a}[1\bar{1}0] + \mathrm{SF}; \qquad (2)$$

We then characterize the 300nm-thick BST film. Fig. 2 (a) is the SAED pattern from a cross-sectional sample of ~ 300 nm thickness along the $[1\bar{1}0]$ zone axis at the interface. According to the XRD results, the thick film is almost fully relaxed. Thus, we expected to observe splitting in the diffraction pattern across the interface. As shown in the inset of Fig. 2 (a), a slightly splitting of $\boldsymbol{g}_{\mathrm{BST}}$ $(22\bar{2})$ and $\boldsymbol{g}_{\mathrm{STO}}$ $(22\bar{2})$ is indicated by the white dashed square. Fig. 2 (b) shows the cross-sectional dark-field TEM image taken along the same zone axis. Overall, the film's thickness is uniform; meanwhile, a high density of threading dislocations, with a reversed 'Y' or 'fork' shape, are observed near the interface. The details of these threading dislocations are discussed later. Figs. 2 (c) and (d) are the FFT-filtered HR-STEM images of the BST film along the $[11\bar{2}]$ zone axis. In Fig. 2 (c), the Burgers vectors of misfit dislocations are observed as $\frac{1}{2}\boldsymbol{a}$<110> with a stacking fault between them indicated by white dashed line. Furthermore, in Fig. 2 (d) we also observed some pairs of misfit dislocations with opposite Burgers

vectors in the thick films, which have been observed in the cubic-on-cubic system as well.[30-32] From the HR-STEM images along $[1\bar{1}0]$ zone axis in Figs. 2 (e) and (f), we observed the perfect misfit dislocation with Burgers vector of $\boldsymbol{a}$<110> as well as two ½$\boldsymbol{a}$<110> type partial dislocations with a stacking fault, which is clearly due to the dislocation dissociation of EQ (2). In principle, there could be an another dissociation reaction of $\boldsymbol{a}$<110> dislocation: $\boldsymbol{a}$<110>= $\boldsymbol{a}$<100>+ $\boldsymbol{a}$<010>, which have been reported in (001)-oriented $BaTiO_3$ and $SrTiO_3$ epitaxial films.[15,17] However, we have not observed this reaction in our system which can be due to that this reaction will not reduce the strain energy. The process of the misfit dislocation reactions can be understood as follows: A $\boldsymbol{a}$<110> dislocation half-loop formed firstly and then the misfit segment dissociates into two partial ones with Burgers vector of ½$\boldsymbol{a}$<110>, and a stacking fault. This reaction may help to relax the dislocation energy of misfit dislocation but increase the stacking fault energy. Therefore, whether the reaction is energetically favorable depends on the area of the stacking fault. It is observed that in Fig. 2 (c) and (e) and Fig. S4, the width of stacking fault is less than 10 nm, which indicates that the existence of stacking faults may couple the ½$\boldsymbol{a}$<110> partial dislocations.

We applied a low angle annular dark-field (LAADF)-STEM electron tomography technique to investigate the 3D structure of threading dislocations in a 300 nm-thick film.[33,34] The LAADF-STEM images were acquired from -65° to 65° with 1° intervals. The 3D reconstruction clearly shows the network of threading dislocations near the interfacial area (Fig. 3 (a) - (d), and Movie 1 in Supplemental Material(Multimedia view)). The as-acquired LAADF-STEM images are shown in Fig. 3 (e) - (g). We observed a high density of threading dislocations with a reversed "Y" shape in the region close to the substrate, as confirmed in the weak-beam dark-field images shown in Fig. S5. At the near surface region of the BST film, we also observed a "Y" shape contrast from the dissociation of the threading dislocations. We note that frequently we observed only two threading dislocations reacting with each other. This might be due to the effect of the local strain field or part of the third threading dislocations was cut off by the FIB.

Each dislocation half-loop is comprised of two threading dislocations, and one segment of misfit dislocation. In our case, the threading dislocations should have the same Burgers vector as misfit dislocations.[26] For the threading segments of the half-loop, though the Burgers vectors remain as $\boldsymbol{a}$<110>, the dislocation lines are tilted to <101>, as indicated by Fig. 1 (b) and (c). As we found from Fig. 3 (e) - (g), the threading dislocations in the film can also interact with each other to relax the strain within the film. All possible reactions between two misfit/threading dislocations are summarized in

Table SI of Supplemental Material. It was supposed that under the compressive strain of BST film on STO, only the misfit dislocations with Burgers vectors along $\boldsymbol{a}[1\bar{1}0]$, $\boldsymbol{a}[\bar{1}01]$ and $\boldsymbol{a}[01\bar{1}]$ are energetically favorable but in reality, we have observed the dislocations with Burgers vectors of $\boldsymbol{a}[\bar{1}10]$, which indicate the strain in BST film is not fully relaxed.

Considering the geometry of the thick film, where the threading dislocations are along <101> and the film normal is [111], we demonstrate five kinds of possible configurations in Fig. 3 (h), based on the TEM results and those from the reconstructed 3D electron tomography. The first one is the case without reactions. The second case describes the reaction observed in Fig. 1 (b) and (c), wherein the dislocation reaction is between misfit dislocations with Burgers vectors of $\boldsymbol{a}[\bar{1}01]$ and $\boldsymbol{a}[01\bar{1}]$. In these two configurations, the threading dislocation part does not react. Since in the (111)-oriented films, the threading dislocation lines orientate along the <110> direction, they can meet and react with each other to form reversed "Y" shape dislocations as shown in the configuration (3) in Fig. 3(h). Among all possible reactions, EQ (3) is likely to be the case because of it is more energetically favorable. For comparison, most threading dislocations in the (001) BST system are along <100>, where they rarely meet and react with each other. Evidenced in Fig. 3, a threading dislocation may undergo a reversed reaction to that of EQ (2) or (4), to dissociate into two threading dislocations at the surface, as shown in configuration (5). In an another case, the reaction of three threading dislocations with Burgers vectors of $\boldsymbol{a}[\bar{1}01]$, $\boldsymbol{a}[01\bar{1}]$, and $\boldsymbol{a}[1\bar{1}0]$ will annihilate themselves in the reaction of EQ (5), and constitute the claw-shaped configuration, shown in configuration (4):

$$\boldsymbol{a}[\bar{1}01] + \boldsymbol{a}[01\bar{1}] = \boldsymbol{a}[\bar{1}10]; \qquad (3)$$

$$\boldsymbol{a}[\bar{1}10] = \boldsymbol{a}[\bar{1}00] + \boldsymbol{a}[\bar{1}00]; \qquad (4)$$

$$\boldsymbol{a}[\bar{1}01] + \boldsymbol{a}[01\bar{1}] + \boldsymbol{a}[1\bar{1}0] = 0; \quad (5)$$

We anticipate the density of configuration (5) would be low because it is supposed to exist only in a fully relaxed sample: any residual stress can result in anisotropy of those three vectors. The configurations of (3), (4) and (5) were experimentally evidenced by the 3D reconstruction shown in Fig. 3, and Movie 1 in Supplemental Material(Multimedia view).

Table I compares the dislocations in (111) epitaxial BST thin film system to those in the (001) epitaxial system. For the (001) epitaxial system, the major dislocations were observed in the {001} planes, with Burgers vector of $\boldsymbol{a}$<100>, whereas we observed both ½$\boldsymbol{a}$<110> and $\boldsymbol{a}$<110> in BST/STO (111) epitaxial films. The threading dislocations in both the (111) epitaxial films and the (001) epitaxial films show the ½$\boldsymbol{a}$<110> and $\boldsymbol{a}$<110> types, respectively. However, we found that the threading dislocations

in the (111) epitaxial films also interact with each other in the lower part, which was seldomly observed in the (001) epitaxial system. This leads to a higher density of threading dislocations near the interface, consequently helping to relax the strain faster in the (111) BST films.[35] Based on this, we believe that the more sufficient strain relaxation in the BST (111) films are responsible for the broadened temperature dependence of permittivity in the (111) BST films, while compared with those in the (001) BST films.

In summary, we investigated the microstructure of the (111) epitaxial BST/STO heterostructure using multiple TEM techniques. We found the dominant dislocation half-loops with Burgers vectors of $\boldsymbol{a}$<110> were comprised of misfit dislocation along <112>, and threading dislocations along <110>. We identified the dissociation of one $\boldsymbol{a}$<110> misfit dislocation into two 1/2$\boldsymbol{a}$<110> partial dislocations and one stacking fault, which consequently leads to the domination of 1/2$\boldsymbol{a}$<110> misfit dislocations. The dislocation reactions occur not only between misfit dislocations but also between threading dislocations using (S)TEM imaging and 3D electron tomography, which lead to a faster strain relaxation in the (111) BST film. Although the dynamic process of the dissociation of the misfit/threading dislocations during the film epitaxy would need further investigations, we believe that our results will give valuable insights into the mechanisms of improving the thin films' physical properties through strain engineering.

Acknowledgements

We thank Drs. A. Wookhead and E. A. Stach for the proof reading. This work is supported by the Center for Functional Nanomaterials, Brookhaven National Laboratory funded by the U.S. Department of Energy, Office of Basic Energy Sciences, under contract no. DE-SC-00112704. XS is grateful for the financial support of the China Scholarship Council and Brookhaven National Laboratory for his exchange program. The work of TY was partially supported by the JSPS KAKENHI Grant No. 20860036 and 22760510, and JST-PRESTO. DW is grateful for financial support from 973 projects of Chinese Ministry of Science and Technology (Grant No. 2015CB921200).

References

[1] M. Stengel, and N. A. Spaldin, Nature **443,** 679 (2006).

[2] D. Nuzhnyy, J. Petzelt, S. Kamba, P. Kužel, C. Kadlec, V. Bovtun, M. Kempa, J. Schubert, C. M. Brooks, and D. G. Schlom, Appl. Phys. Lett. **95,** 232902 (2009).

[3] N. Setter, D. Damjanovic, L. Eng, G. Fox, S. Gevorgian, S. Hong, H. Kohlstedt, A. Kingon, N. Y. Park, G. B. Stephenson, *et al.,* J. Appl. Phys. 100, 051606 (2006).

[4] G. A. Samara, E. L. Venturini, and V. Hugo Schmidt, Appl. Phys. Lett. 76, 1327 (2000).

[5] T. Yamada, K. F. Astafiev, V. O. Sherman, A. K. Tagantsev, D. Su, P. Muralt, and N. Setter, J. Appl. Phys. 98, 054105 (2005).

[6] A. Noeth, T. Yamada, V. O. Sherman, P. Muralt, A. K. Tagantsev, and N. Setter, J. Appl. Phys. 102, 114110 (2007).

[7] C. L. Canedy, Hao Li, S. P. Alpay, L. Salamanca-Riba, A. L. Roytburd, and R. Ramesh, Appl. Phys. Lett. **77,** 1695 (2000).

[8] Hao Li, A. L. Roytburd, S. P. Alpay, T. D. Tran, L. Salamanca-Riba, and R. Ramesh, Appl. Phys. Lett. **78,** 2354 (2001).

[9] B. H. Park, E. J. Peterson, Q. X. Jia, J. Lee, X. Zeng, W. Si, and X. X. Xi, Appl. Phys. Lett. **78,** 533 (2001).

[10] Z. -G. Ban, and S. P. Alpay, J. Appl. Phys. **91,** 9288 (2002).

[11] Z. -G. Ban, and S. P. Alpay, J. Appl. Phys. **93,** 504 (2003).

[12] X. Shen, K. Ahmadi-Majlan, J. H. Ngai, D. Wu, and D. Su, Appl. Phys. Lett. **106,** 032903 (2015).

[13] J. W. Matthews, and A. E. Blakeslee, J. Cryst. Growth **27,** 118 (1974).

[14] R. People, and J.C. Bean, Appl. Phys. Lett. **47,** 322 (1985).

[15] T. Suzuki, Y. Nishi, and M. Fujimoto, Philos. Mag. A **79,** 2461 (1999).

[16] D. Su, T. Yamada, V. O. Sherman, A. K. Tagantsev, P. Muralt, and N. Setter, J. Appl. Phys. **101,** 064102 (2007).

[17] Y. L. Qin, C. L. Jia, K. Urban, J. H. Hao, and X. X. Xi, J. Mater. Res. **17,** 3117 (2002).

[18] C. J. Lu, L. A. Bendersky, K. Chang, and I. Takeuchi, J. Appl. Phys. **93,** 512 (2003).

[19] H.-J. Gao, C. L. Chen, B. Rafferty, S. J. Pennycook, G. P. Luo, and C. W. Chu, Appl. Phys. Lett. **75,** 2542 (1999).

[20] M. -W. Chu, I. Szafraniak, R. Scholz, C. Harnagea, D. Hesse, M. Alexe, and U. Gösele, Nature Mater. **3,** 87 (2004).

[21] V. Nagarajan, C. L. Jia, H. Kohlstedt, R. Waser, I. B. Misirlioglu, S. P. Alpay, and R. Ramesh, Appl. Phys. Lett. **86,** 192910 (2005).

[22] O. Nakagawara, T. Shimuta, T. Makino, S. Arai, H. Tabata, and T. Kawai, Appl. Phys. Lett. **77,** 3257 (2000).

[23] T. Yamada, T. Kamo, H. Funakubo, D. Su, and T. Iijima, J. Appl. Phys. **109,** 091605 (2011).
[24] H. P. Sun, X. Q. Pan, J. H. Haeni, and D. G. Schlom, Appl. Phys. Lett. **85,** 1967 (2004).
[25] D. Su, Q. P. Meng, C. A. F. Vaz, M.-G. Han, Y. Segal, F. J. Walker, M. Sawicki, C. Broadbridge, and C. H. Ahn, Appl. Phys. Lett. **99,** 102902 (2011).
[26] I. A. Ovid'ko, J. Phys.: Condens. Matter **11,** 6521 (1999).
[27] H. M. Christen, E. D. Specht, S. S. Silliman, and K. S. Harshavardhan, Phys. Rev. B **68,** 020101(R) (2003).
[28] A.C. Dent, C.R. Bowen, R. Stevens, M.G. Cain, and M. Stewart, J. Eur. Ceram. Soc. **27,** 3739 (2007).
[29] D. Hull, and D. J. Bacon, *Introduction to dislocations* (Elsevier, Oxford, ed. 5, 2011), pp. 73.
[30] G.Y. Yang, J.M. Finder, J. Wang, Z.L. Wang, Z. Yu, J. Ramdani, R. Droopad, K.W. Eisenbeiser, and R. Ramesh, J. Mater. Res. **17,** 65 (2002).
[31] C. J. Lu, L. A. Bendersky, K. Chang, and I. Takeuchi, Philo. Mag. **83,** 1565 (2003).
[32] Sung Bo Lee, Wilfried Sigle, Fritz Phillipp, and Dieter Brunner, Acta Materialia **53,** 1843 (2005).
[33] J. S. Barnard, J. Sharp, J. R. Tong, and P. A. Midgley, Philos. Mag. **86,** 4901 (2006).
[34] K. He, H. L. Xin, K. Zhao, X. Yu, D. Nordlund, T. -C. Weng, J. Li, Y Jiang, C. A. Cadigan, R. M. Richards, *et al.,* Nano Lett. **15,** 1437 (2015).
[35] D. Su, T. Yamada, R. Gysel, A. K. Tagantsev, P. Muralt, N. Setter, and N. Jiang, J. Mater. Res. **26,** 770 (2011).
[36] See supplemental material at [URL] for plane-view images of (100)-oriented films, STEM-EELS line-scan result, weak-beam dark-field images, and 3D reconstructed tomogram.

Figure Captions

Figure 1. TEM results of the (111) BST (10nm)/STO heterostructure (a) Plane-view SAED pattern. (b) Plane-view bright- field images of BST film under the two-beam condition, with $\boldsymbol{g} = 10\bar{1}$. (c) Two enlarged images from the selected area of (b), marked with green and blue squares respectively. The schematic figure also is shown. (d) Cross-sectional SAED pattern along $[11\bar{2}]$ zone axis. FFT-filtered HRTEM image at $(11\bar{2})$ plane (e) and FFT-filtered HRSTEM image along $[1\bar{1}0]$ zone axis (f). The Burgers circuit is drawn around the dislocation core. (g) Schematic diagram of the Burgers vectors of $\boldsymbol{a}$ <110> and $\boldsymbol{\frac{1}{2}a}$ <110> in <111> plane. (Sr: green, Ti: light blue, O: red)

Figure 2. TEM results of the (111) BST (300nm) film on STO (a) Cross-sectional SAED pattern. (b) Dark-field TEM image of the BST film under the two-beam condition, with $\boldsymbol{g} = 1\bar{1}0$. FFT-filtered HRSTEM images along $[11\bar{2}]$ zone axis are shown in (c) and (d). FFT-filtered HRSTEM images along $[1\bar{1}0]$ zone axis are shown in (e) and (f). The stacking faults are indicated by the white dashed lines. The Burgers circuit is drawn around the dislocation core.

Figure 3. A series of reconstructed 3D tomograms from the interface between BST film (300nm) and STO substrate at viewing angles of 0° (a), 45° (b), 90° (c) and 135° (d) (Multimedia view). The original LAADF-STEM images during the recording at view angles of -29.3° (e), -0.1° (f) and 28° (g). Scale bar is100 nm. (h) The schematic diagram of the configurations of the misfit (blue and dash lines) and the threading (red and solid lines) dislocation network in BST films.

Table I. The Burgers vectors and dislocation lines of misfit and threading dislocations in (001) and (111) epitaxial films.

Dislocation Type	(100) BST on (001) STO	(111) BST on (111) STO
Misfit dislocation	$\boldsymbol{b} = \boldsymbol{a}\langle 100\rangle$; $\boldsymbol{l} = \langle 100\rangle$	$\boldsymbol{b} = \frac{1}{2}\boldsymbol{a}\langle 110\rangle$ or $\boldsymbol{a}\langle 110\rangle$; $\boldsymbol{l} = \langle 112\rangle$
Threading dislocation	$\boldsymbol{b} = \frac{1}{2}\boldsymbol{a}\langle 110\rangle$ or $\boldsymbol{a}\langle 110\rangle$; $\boldsymbol{l} = \langle 001\rangle$	$\boldsymbol{b} = \frac{1}{2}\boldsymbol{a}\langle 110\rangle$ or $\boldsymbol{a}\langle 110\rangle$; $\boldsymbol{l} = \langle 110\rangle$ or $\langle 100\rangle$

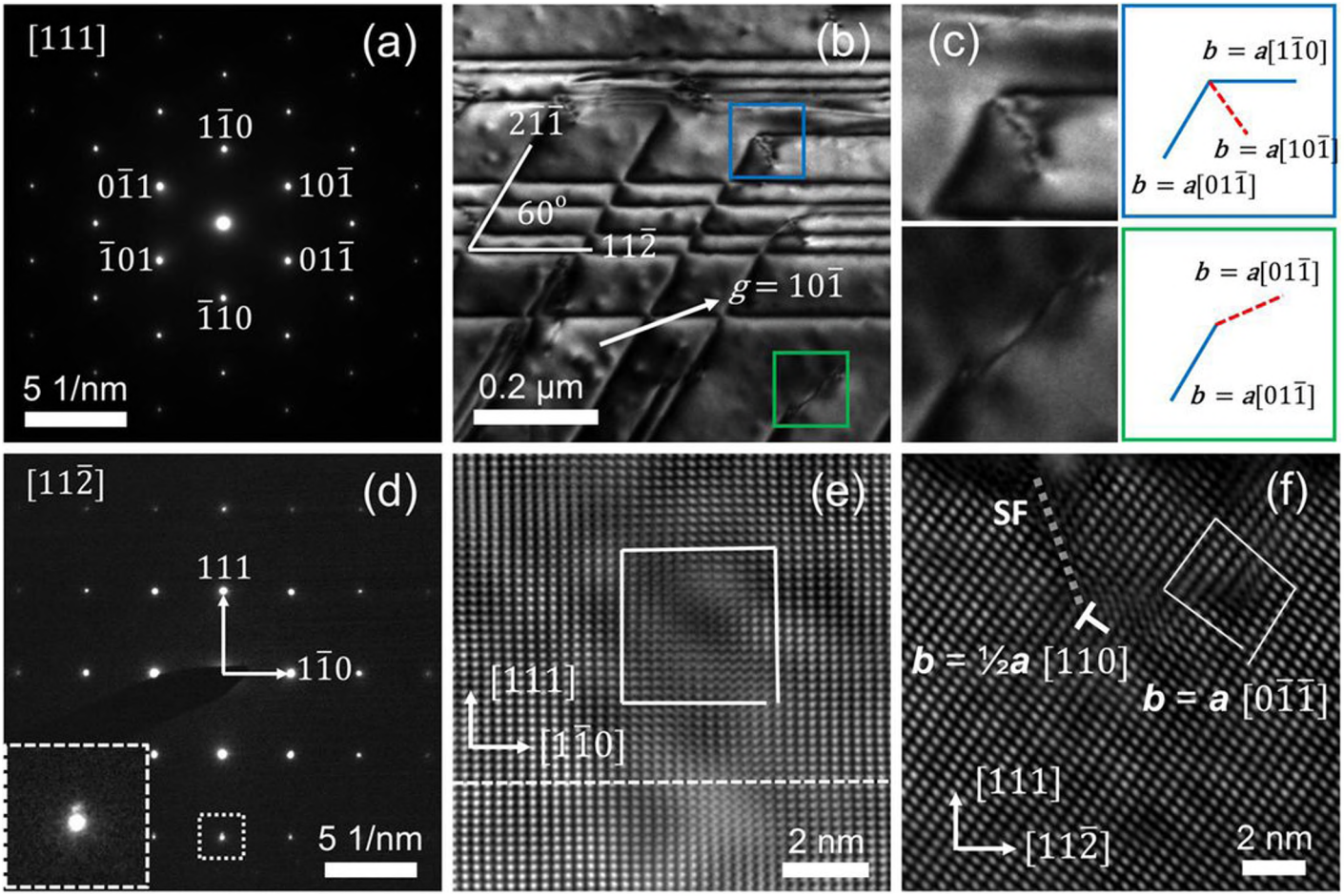
[111]
(a)
1$\bar{1}$0
0$\bar{1}$1
10$\bar{1}$
$\bar{1}$01
01$\bar{1}$
$\bar{1}$10
5 1/nm
(b)
21$\bar{1}$
60°
11$\bar{2}$
g = 10$\bar{1}$
0.2 μm
(c)
b = a[1$\bar{1}$0]
b = a[10$\bar{1}$]
b = a[01$\bar{1}$]
b = a[01$\bar{1}$]
b = a[01$\bar{1}$]
[11$\bar{2}$]
(d)
111
1$\bar{1}$0
5 1/nm
(e)
[111]
[1$\bar{1}$0]
2 nm
(f)
SF
b = ½a [110]
b = a [0$\bar{1}$$\bar{1}$]
[111]
[11$\bar{2}$]
2 nm

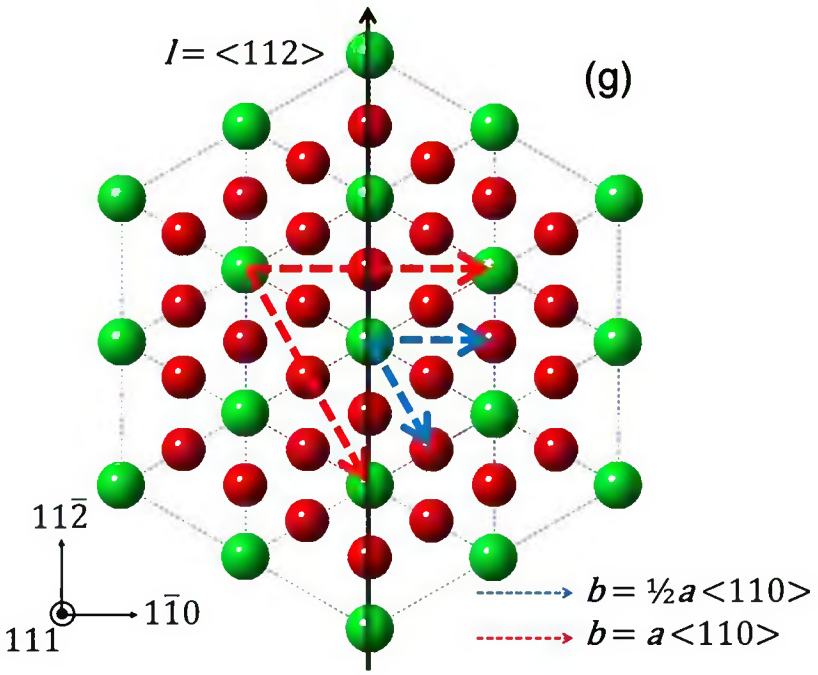
l = <112>
(g)
11$\bar{2}$
1$\bar{1}$0
111
b = ½a <110>
b = a <110>

Figure 1

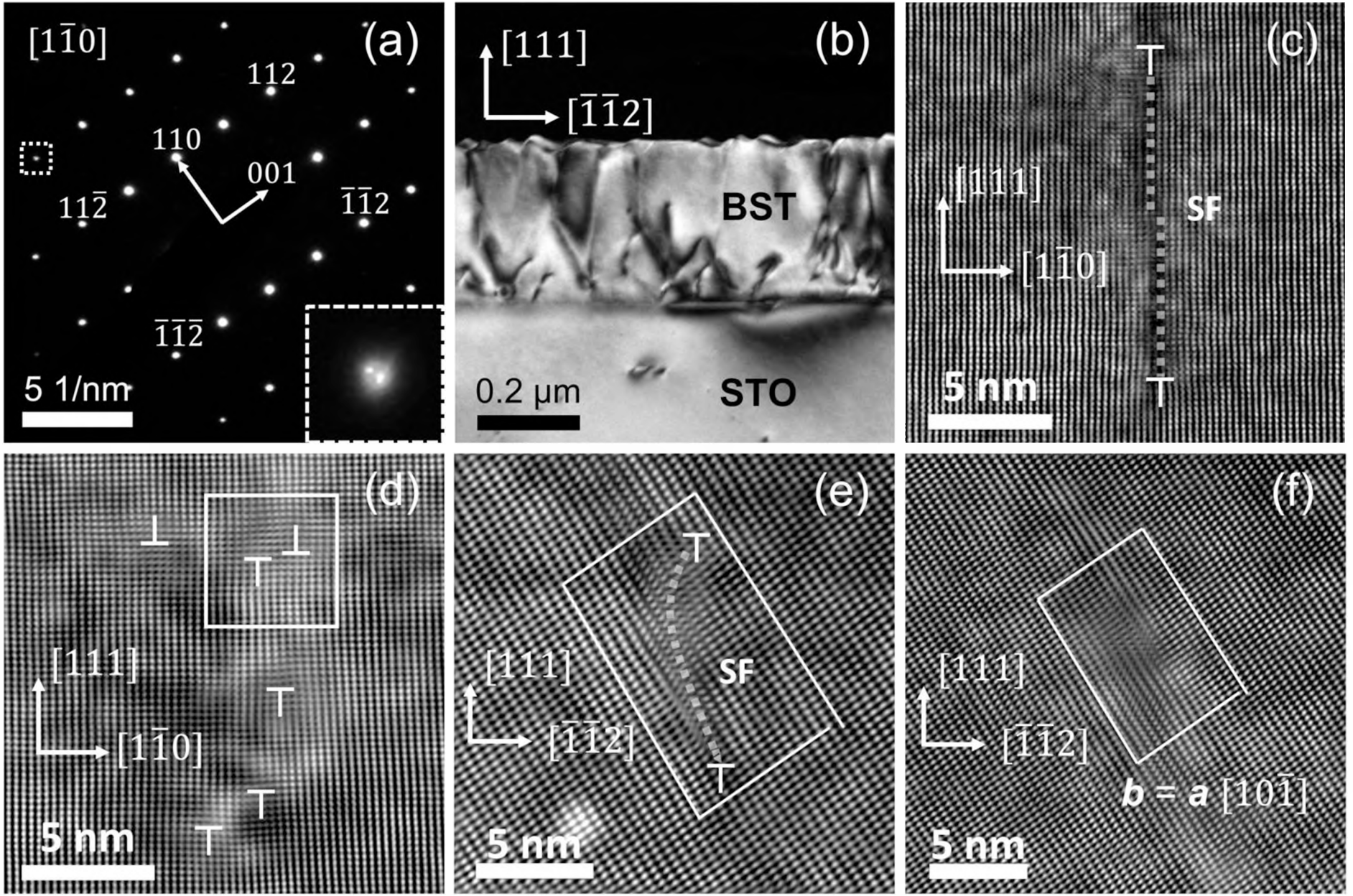
[1$\bar{1}$0]
(a)
112
110
001
11$\bar{2}$
$\bar{1}\bar{1}$2
$\bar{1}\bar{1}\bar{2}$
5 1/nm
[111]
(b)
[$\bar{1}\bar{1}$2]
BST
0.2 μm
STO
T
(c)
[111]
[1$\bar{1}$0]
SF
5 nm
T
(d)
⊥
T
⊥
[111]
[1$\bar{1}$0]
T
T
T
5 nm
(e)
T
[111]
SF
[$\bar{1}\bar{1}$2]
T
5 nm
(f)
[111]
[$\bar{1}\bar{1}$2]
b = a [10$\bar{1}$]
5 nm

Figure 2

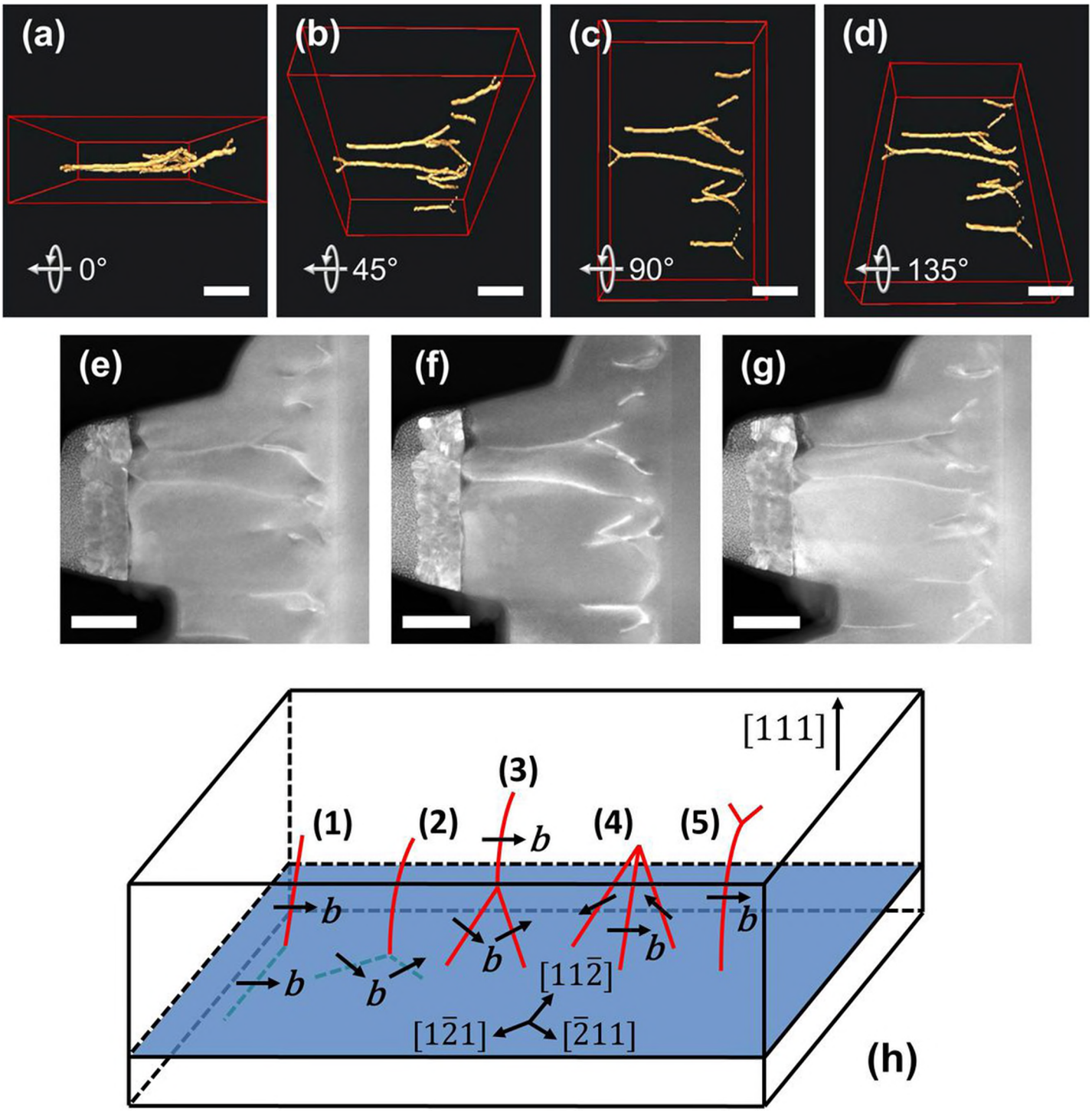

Figure 3